UNIVERSAL WISER
PUBLISHER

Research Article

Multifractal Analysis on Ozone Depletion and Climate Change: The Time Series Approaches

M. Meenakshi![ID], A. Gowrisankar*![ID]

Department of Mathematics, School of Advanced Sciences, Vellore Institute of Technology, Vellore, 632014, Tamil Nadu, India
E-mail: gowrisankargri@gmail.com

Abstract: The ozone layer has acted as the planet's natural sunscreen, protecting people, plants, and animals from harmful ultraviolet rays. The Antarctic ozone hole was first announced in a paper by the British Antarctic Survey's Joe Farman, Brian Gardiner, and Jonathan Shanklin in 1985. Many investigations are still conducting to determine the connection between ozone depletion and climate change. This research study investigates the impact of the ozone layer's depletion at the Antarctic pole on global climate change data such as temperature and precipitation, after the year 1985 through a fractal dimension, Multifractal Detrended Fluctuation Analysis (MFDFA), and standard correlation coefficient. For this, the research work has analyzed 45 years of climate change variables such as global monthly temperature anomaly, global monthly precipitation anomaly, and Southern Hemisphere minimum ozone time series data from 1979 to 2023. The fractal dimension of the time series is obtained by rescaled range analysis, which is used to identify the fractality of the time series and long-range correlations and persistence. To study the multifractality of these fractal time series, MFDFA procedure has been applied. By applying MFDFA to these time series data, this research has identified significant multifractal characteristics, indicating complex dynamics and long-range correlations, and identified potential nonlinear patterns. This research provides valuable insights into the complex dynamics of time series data, as revealed by the calculated exponent values and MFDFA spectrum. The strong correlation observed between the exponent values of temperature anomalies, and precipitation anomalies, with ozone depletion time series provides compelling evidence for the significant impact of ozone depletion on climate change. These results highlight the potential of multifractality for understanding the intricate mechanisms underlying climate change.

Keywords: climate change, ozone depletion, fractal dimension, multifractal detrended fluctuation analysis, correlation coefficient

MSC: 28A80, 62M10

Abbreviation

H	Hurst Exponent
FD	Fractal Dimension
GMTA	Global Monthly Temperature Anomaly
GMPA	Global Monthly Precipitation Anomaly
$SHMO_3$	Southern Hemisphere Minimum Ozone
MFDFA	Multifractal Detrended Fluctuation Analysis

1. Introduction

Long-term changes in the climate that have taken place over decades, centuries, or longer have been referred to as climate change. All creatures on Earth have become aware of climate change through multiple disasters like intense rain, high temperatures, heat waves, landslides, floods, and so on. Global warming has raised interest in climate change studies during the last few decades. Many of the factors influencing climate change have been identified on Earth. Among many factors, greenhouse gases have been recognized as the primary contributors to increasing global warming. Scientists have also been searching for the causes of climate change above the surface of the Earth, especially space-related factors. Therefore, the researchers have been searching for the factors from the atmosphere.

The atmosphere has been described as a blanket of gases that surrounds the Earth. It has been made up of a mixture of gases, mostly nitrogen, oxygen, argon, and carbon dioxide. It has reached over 500 km above the surface of the planet. The atmosphere contains many layers. The stratosphere is one of the atmospheric layers, lying between 12 to 50 kilometers above the Earth's surface, and contains the natural ozone (O_3) layer. Ozone has been identified as a gas made up of three oxygen atoms (O_3). The ozone layer in the stratosphere has been absorbing most of the sun's ultraviolet (UV) radiation. A hole in the ozone layer over Antarctica has been discovered by the British Antarctic Survey's Joe Farman, Brian Gardiner, and Jonathan Shanklin, and it was announced in 1985 [1]. The Antarctic ozone hole is an event where the ozone concentration over Antarctica becomes significantly depleted during the Southern Hemisphere's springtime (September-November). This depletion is mainly caused by human-made chemicals called chlorofluorocarbons (CFCs), which are commonly used in air conditioners, refrigerators, fire extinguishers, aerosols, and other goods. Usually, these goods are referred to as ozone-depleting substances (ODS) [2].

This ozone is measured in units called Dobson Units (DU). Dobson Unit has referred to the thickness of the ozone layer in a vertical column from the surface to the top of the atmosphere, a quantity called the "total column ozone amount". Before 1979, total column ozone values over Antarctica had never depleted below 220 Dobson Units (DU). The global mean ozone concentration in the upper atmosphere is around 300 DU, with regional variations ranging from 230 to 500 DU. Ozone in the total column rises with latitude and has an average minimum throughout the equatorial belt. The region where ozone column values are equal to or less than 220 DU is commonly referred to as the ozone hole.

Ozone depletion has referred to two phenomena: a decrease in the overall amount of ozone in the stratosphere and a drop in ozone on the pole side during the long springtime [3–6]. Figure 1 represents the layers of the atmosphere along with the ozone layer in the stratosphere and ozone depletion over Antarctica. This ozone hole has become a global issue. The scientists have made awareness about the ozone hole to governments, and have made efforts to stop it. As a result, Mostafa Kamal Tolba, head of the United Nations Environment Programme (UNEP), brought the nations together for a global agreement to safeguard the stratospheric ozone layer. This agreement was signed in 1987 and has called the Montreal Protocol, which has gradually ceased the manufacturing and use of ozone-depleting substances (ODS). It has been ratified by 197 countries, making it the first treaty in the history of the United Nations to achieve universal ratification. The protocol has been successful in reducing the atmospheric concentrations of key ODS, such as chlorofluorocarbons (CFCs) and halons, by over 90% since its implementation [7].

Many researchers have been attempting to determine the association between the ozone hole and climate change. Nowadays, researchers have preferred to work on meteorological phenomena, especially temperature and precipitation data in the anomalies, rather than absolute values. An anomaly refers to a deviation from the expected or typical pattern or behavior. Temperature (or precipitation) anomalies typically represent deviations from the long-term average or

climatological norm for a given location and period. Temperature anomalies have indicated whether temperatures have been higher or lower than average for a specific period, while precipitation anomalies have indicated whether precipitation amounts have been above or below average. These have been used to understand and monitor climate variability and change, as well as to estimate the impacts of weather events such as heatwaves, droughts, heavy rainfall, and so on [8].
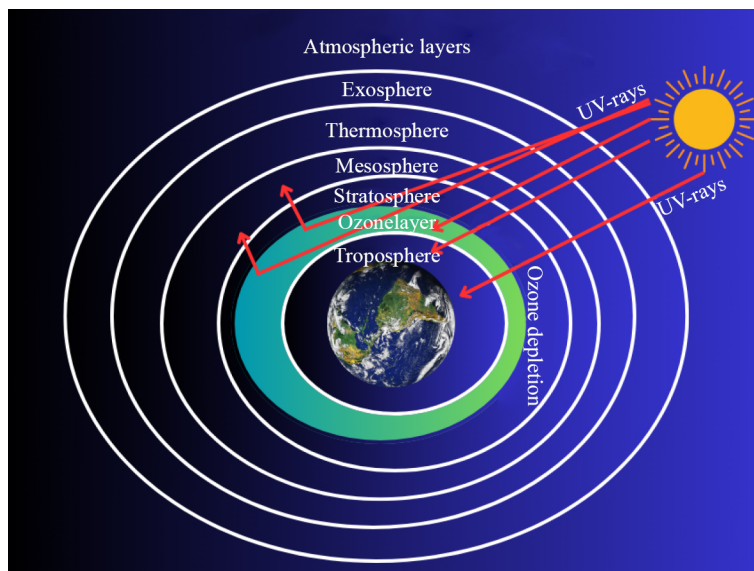

Figure 1. Ozone depletion in the stratosphere

Researchers have used many different tools and models for their research. Ozone depletion has been analyzed by the authors of the article [9] using mathematical models, particularly the weighted multiplicative algebraic reconstruction technique. In the article [10], the authors have discussed how the mathematical model has been crucial as it has allowed for simulating ozone depletion phenomena through chemical kinetics and Ordinary Differential Equations (ODEs), providing insights into concentration variations of stratospheric elements. This has aided ozone monitoring stations in predicting future atmospheric changes effectively. In the article [11], the mathematical model has been essential in assessing the impact of temperature increases caused by greenhouse gases like CFC on prey-predator dynamics. Using stability theory, it has provided a threshold stress parameter to predict the survival or extinction of populations, offering valuable insights into ecosystem stability. The mathematical model has been pivotal in improving the accuracy of Taiwan's daily maximum ozone concentration predictions by utilizing a two-stage fuzzy time series approach in the article [12]. It has outperformed traditional models, providing enhanced tools for assessing air quality and addressing environmental concerns. In [13], the authors have used the short-term variability method to analyze the Antarctic ozone hole, sea surface temperature, surface temperature, and zonal wind. They have concluded from their result that the ozone hole-related surface wind anomalies have caused cooling across the Southern Ocean, which might have impacted temperatures in the eastern tropical Pacific. In the article [14], the authors have used satellite data and passive-tracer methods to examine ozone loss in the Antarctic over eight years 2013 to 2020. They have identified that the highest ozone loss in 2020 was due to high chlorine levels and a stable polar vortex. In the article [15], the authors have discussed the time series of airborne observation of ozone and meteorological quantities with fractal geometry and Hurst exponent. As a result, they have suggested that ozone and horizontal wind speed have behaved as random, self-affine fractals and multifractality is present in the persistent variables. In the article [16], the authors have discussed the complexity of analyzing environmental phenomena like atmospheric pollution, temperature variability, global warming, and ozone layer depletion (OLD) using deterministic models. Their study has introduced time series modeling to analyze the fluctuating dynamics of the ozone layer and has employed techniques like bi-spectrum analysis and correlation dimension to understand the chaotic nature of OLD.

The concept of multifractality has found widespread application across various fields. Researchers have identified multifractality using a range of tools, including Detrended fluctuation Analysis (DFA), Multifractal Detrended fluctuation Analysis (MFDFA), Multifractal Detrended Cross-Correlation Analysis (MF-DCCA), and wavelet transform, among others. In continuation, the authors of the paper [17] have used wavelet and detrended fluctuation analysis techniques for non-stationary data of total column ozone to detect long-range correlation. Their results have shown that column ozone fluctuations exhibit persistent long-range power-law correlations for all-time lags between 4 months and 11 years. The ozone research with modern techniques has continued with the 10-minute ozone concentration time series from Cordoba in 2007 has been examined by the authors of the paper [18] using multifractal analysis to comprehend its seasonal patterns and multifractal character. Beyond conventional statistical techniques, multifractal analysis has provided extensive insights into the structure of ozone time series by revealing heterogeneity. So, the multifractal detrended fluctuation analysis (MFDFA) has become a widespread technique to find the complexity and multifractality of the variables. Many researchers have been utilizing the MFDFA as a tool for their research.

In the sequence, the authors of the article [19] have utilized multifractal detrended fluctuation analysis (MFDFA) on a daily time series spanning 31 years from stations across Europe to analyze the scaling properties of agro-meteorological factors. Their results have revealed a multifractal structure with diverse dynamics across variables. And they have suggested that the MFDFA has an effective technique for offering insights into the effectiveness of climate dynamics. Following that, MFDFA has been applied by the researchers of the article [20] to daily total ozone concentration (TOC) data for the years 2015 to 2019. It has been possible to identify multifractal behavior and obtain a generalized Hurst exponent larger than 0.5.

In [21], they have analyzed that hierarchical organization is central to complexity, with multifractality as its key quantifying concept. While model cascades show symmetric singularity spectra, empirical data often exhibit asymmetric spectra. Examples include financial markets, narrative text variability, and Sunspot Number fluctuations, where asymmetry, particularly in Sunspot data, suggests either distortion by the Wolf formula or a different underlying dynamic mechanism. In this order, the analysis of multifractality has been employed in many time series like Southern Oscillation Index [22], the presence of natural radionuclides in the atmosphere and water [23], a study of ozone, pollutants like NO_x, SO_2, and surface temperature in Kolkata's pre-lock-down (2019) and lock-down (2020) periods [24], the impact of COVID-19 lock-downs on air quality in the Hong Kong port area [25], the time series of total ozone concentrations in New Delhi [26]. Investigation of $PM_{2.5}$ and PM_{10} Dynamics in the Caribbean Basin [27], multifractality analysis of fractal interpolation functions [28], time series analysis of Mpox outbreak [29]. The multifractal analysis has been extended to the joint multifractal analysis. This technique has been used for three variables, temperature, NO_2, and ozone, that coexist in the same geometric support in the paper [30]. Scale-dependent interactions among variables have been shown by joint multifractal analysis conducted on hourly data from Seville in the summer of 2011. They have obtained the result that the temperature has significantly impacted ozone concentrations across time scales.

Literature reviews have shown that multifractal analysis, particularly through the MFDFA procedure, has been crucial for understanding multifractal behavior in climate systems. MFDFA has been recognized as a robust tool for analyzing the complex, scale-dependent variability in atmospheric data. This approach has enabled a better understanding of the mechanisms governing climate variability and ozone depletion, which are critical for predicting long-term trends and addressing environmental challenges [31]. These qualities of MFDFA have inspired us to use it for studying climate change.

We have analyzed climate changes considering various influencing factors. In a previous study [32], we examined the impact of carbon dioxide on temperature and precipitation. Now, we have turned our focus to studying the effects of ozone depletion on climate change using multifractal analysis. MFDFA has been chosen for its robustness in analyzing complex time series and its ability to detect multifractal properties, making it ideal for exploring the dynamics of non-stationary data.
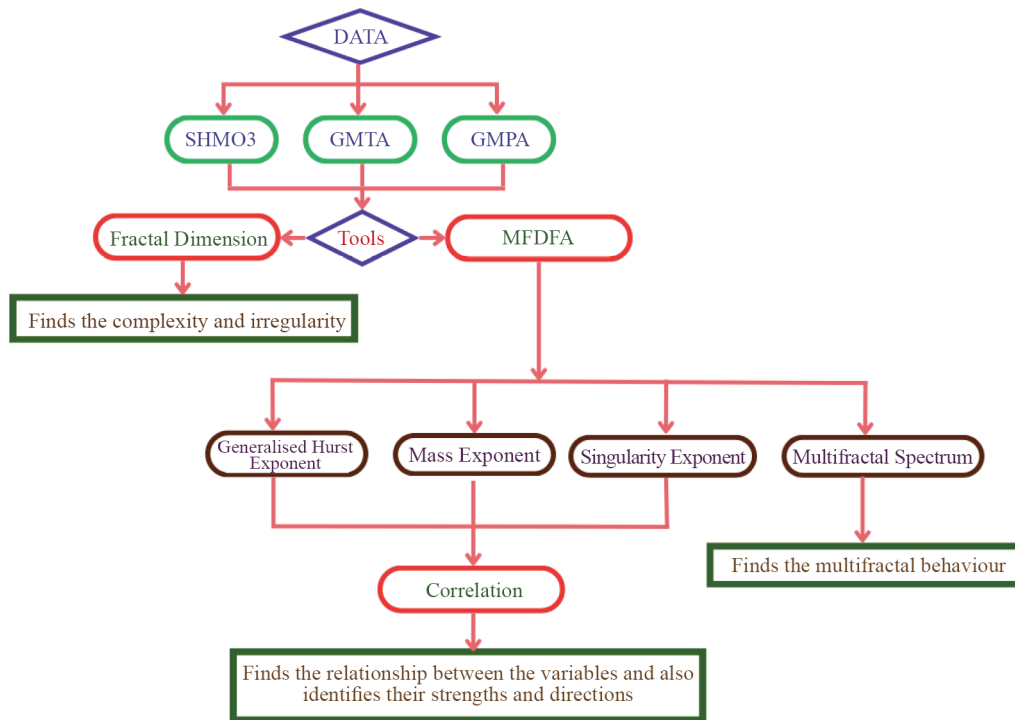
Figure 2. Schematic diagram

By leveraging the fractal dimension as an analytical tool, this study has provided deeper insights into the scaling properties and multifractal nature of the time series. The fractal dimension, derived from the Hurst exponent ($D = 2 - H$), has indicated the sources of multifractality in chosen datasets like $SHMO_3$, GMTA, and GMPA. Non-integer fractal dimension values have revealed the fractal nature of the data, which has been fundamental to identifying multifractal characteristics. This has strengthened our commitment to using the MFDFA procedure.

While substantial research has focused on ozone depletion and climate change individually, no study has yet explored the time-series data of ozone depletion in the Southern Hemisphere alongside global climate variables such as temperature anomalies and precipitation anomalies. This work has employed analytical tools like fractal dimension, MFDFA exponents, their spectrum, and standard correlation coefficients. This study has represented a significant effort to address this gap, providing a novel perspective on the intricate relationship between ozone depletion and climate change. By doing so, it has held the potential to enrich our understanding of their interconnected dynamics. The key contributions and novel aspects of this research are summarized as follows: This study has introduced a novel approach by employing fractal dimension, MFDFA procedure, and standard correlation coefficient to examine the impact of ozone depletion on global temperature and precipitation anomalies.

• It has emphasized the complexity and persistence of these climate variables from 1979 to 2023, with a particular focus on the post-1985 period, when ozone depletion has accelerated and has begun to influence climate patterns.

• By integrating fractal dimension, MFDFA exponents and their spectrum, and correlation coefficients, this research has offered a unique perspective on the interdependence between changes in ozone depletion and global climate anomalies. To aid in understanding the overall approach, this study has presented a Schematic diagram in Figure (2).

The article has been organized as follows: Section 2 has outlined the methodologies employed in this work, while Section 3 describes the data collection process and provides an overview of the dataset. Section 4 has discussed the results, Section 5 has addressed the research limitations and has suggested potential directions for future work, and Section 6 concludes the study by summarizing the key findings.

2. Methods and materials

This research has utilized the following methods:
• Rescaled Range analysis
• Fractal Dimension
• Multifractal Detrended Fluctuation Analysis (MFDFA)
• Correlation coefficient.

2.1 *Rescaled range analysis*

To calculate the Hurst Exponent using rescaled range analysis, the non-stationary time series X_k has been divided into segments X_t, where the segment lengths are powers of two, and t has varied from $1, 2, \ldots, N$. The time series has been split into s non-overlapping subintervals of equal length, where s is the segment length. The mean of the data for each segment has been calculated as $\bar{X}_t = \frac{1}{s} \sum_{i=1}^{s} X_i$, where t is the segment index and X_i represents the data points within that segment. To, detrend the data, the mean $\bar{X}_t$ of the segment has been subtracted from each data point X_i within the segment to obtain the deviations $Y_i = X_i - \bar{X}_t$ for $t = 1, 2, \ldots, N$. This step represents the fluctuation around the mean. Next, calculate the cumulative sum of deviations for each point within the segment has been calculated as $y_i = \sum_{j=1}^{i} Y_j$, where i runs over the data points in the segment. After this, find the range of the cumulative sum for each interval $R_i = \max(y_i) - \min(y_i)$ for $i = 1, 2, \ldots, s$. The standard deviation for each segment has been calculated as $\sigma_s = \sqrt{(\frac{1}{s} \sum_{i=1}^{s} (X_i - \bar{X}_t)^2)}$ where s is the segment length. Finally, the range has been divided by the standard deviation for each segment as $(R/S)_s = \frac{R_s}{\sigma_s}$ where s is the segment length. Logarithmic scaling has been applied to both R/S and s, which has resulted in a straight line on a $log - log$ plot. Then fit a linear regression to the plot $log(s)$ vs $log(R/S)$. The slope of this fit line has been a Hurst exponent H. If the Hurst exponent value has fallen between $0 < H < 0.5$, then it has indicated anti-persistence, meaning that an increase in value is more likely to be followed by a decreased value, reflecting short range correlations. If $H = 0.5$, it has represented a random walk, indicating the absence of correlations and making future values unpredictable. If the Hurst exponent value has fallen between $0.5 < H < 1$, it has indicated persistence, meaning that an increase in value is likely to be followed by another increase, reflecting long-range correlations [33].

2.2 *Fractal dimension*

From this Hurst exponent value, one can find the fractal dimension easily. A fractal is an object, a curve, or a pattern that keeps repeating at any scale indefinitely. It has a self-similar pattern with unlimited complexity at various sizes. The fractal has been classified into two categories due to its self-similarity: random fractals and deterministic fractals. Random fractals are statistically self-similar; deterministic fractals are exactly self-similar. Numerous natural examples, such as lightning, coastlines, and tree branches, have been classified as random fractals. The Cantor set, the Sierpinski gasket, and Menger's sponge have been a few examples of deterministic fractals. All fractal objects have non-integer dimensions. The fractal has no proper definition, even though Mandelbrot, known as the father of fractals defined it as "a set for which the Hausdorff-Besicovitch dimension strictly exceeds the topological dimension" [34, 35]. Many different methods have been used to obtain the fractal dimension. To find the fractal dimension from the Hurst exponent value, Mandelbrot has developed the formula as

$$FD = E + 1 - H \tag{1}$$

where FD is the fractal dimension, E is the Euclidean dimension, and H is the Hurst exponent. The Euclidean dimension has $E = 0$ for a point, 1 for a line, and 2 for a surface. Whenever H has less than 1, then the object intrudes into the next

dimension, just as a curve or rough surface requires embedding in 3-D space to be visualized. The Euclidean dimension for time series data is one. Therefore, the equation 1 becomes

$$FD = 2 - H. \tag{2}$$

Thus the formula, equation 2 has been used to find the fractal dimension through the Hurst exponent for one-dimension objects [36].

2.3 *Multifractal detrended fluctuation analysis (MFDFA)*

Multifractal is a measure to quantify the fractal datasets. Multi-fractal analysis has become a powerful method of characterizing long-range correlations within time series through the calculation of different scaling exponents for different parts of the series [37–41]. The multifractal detrended fluctuation analysis (MFDFA) extension of the Detrended fluctuation analysis (DFA) model has made it possible to unfold the scaling behavior of the fluctuations in the time series and find the spectrum of singularities. This has been formulated and spread by Kantelhardt et al. in [42]. A multifractal system has become a generalization of a fractal system. Unlike traditional fractals, which have a single exponent (the fractal dimension) to describe their dynamics, multifractal systems have many exponents to describe the complexity, irregularity, and persistence at different scales. Examples of multifractal systems in nature are coastlines, mountain topography, fully developed turbulence, real-world scenes, heartbeat dynamics, human gait, brain activity, and many more.

The MFDFA has exhibited scaling properties across multiple scales. By analyzing the fluctuations in the data across different scales, MFDFA has offered insights into the underlying complexity and organization of the dataset. In MFDFA, relationships between variables have often been inferred from the scaling properties observed across various scales. The scaling exponent derived from MFDFA has provided insights into their relationships. Essentially, if two variables have demonstrated similar scaling exponents across different scales, then it suggests they have shared similar underlying dynamics or structures. Conversely, differences in scaling exponents have indicated different underlying processes or relationships between the variables [43, 44].

Multifractal spectrum analysis has been another method used to characterize the multifractal properties of a dataset. It has quantified the distribution of singularity exponents, which has described the local scaling behavior of the data across different scales. To describe the dynamics, multifractal systems have required a continuous spectrum of exponents known as the singularity spectrum. The behavior around any point has been described by a local power law. The exponent in this power law has been called the singularity exponent, which characterizes the local degree of singularity or regularity around the point. The ensemble of points sharing the same singularity exponent has formed the singularity manifold, which is a fractal set. The curve representing the relationship between singularity exponents and their measure has been called the singularity spectrum.

It has fully described the statistical distribution of the variable in the multifractal system. By distorting datasets extracted from patterns, a multifractal spectrum has been generated. The spectrum has illustrated how scaling varies across the dataset. Both MFDFA exponents and multifractal spectrum analysis have provided valuable insights into the relationships between variables by characterizing their scaling properties and multifractal structures. The MFDFA concepts and their various applications have been understood from the article [42].

The MFDFA has comprised five steps, with the first three steps having employed a conventional DFA procedure. Let's assume that x_k has been a series of length N, and the series has exhibited compact support, i.e., x_k has equaled zero for only an insignificant fraction of the values.

• The profile $Y(i)$ has been determined by subtracting the mean value and integrating the time series, which has converted the noises into random walks.

$$\mathbf{Y(i)} \equiv \sum_{k=1}^{i} [\mathbf{x_k} - \bar{\mathbf{x}}], \; i = 1, \, 2, \, 3, \, \ldots, \, N \tag{3}$$

where $\bar{\mathbf{x}}$ is the mean of the series.

- The profile $\mathbf{Y(i)}$ has been divided into

$$N\mathbf{s} \equiv int(N/\mathbf{s}) \tag{4}$$

non-overlapping segments of equal length $\mathbf{s}$.

- To avoid bias at the edges, the process has been repeated starting from the opposite end of the profile, resulting in $2N_\mathbf{s}$ segments.
- The least square fit technique has been applied to the series to determine the local trend for each of the $2N_\mathbf{s}$ segments. Then, the variance has been found as:

$$\mathbb{F}^2(\nu, \, \mathbf{s}) \equiv \frac{1}{\mathbf{s}} \sum_{i=1}^{\mathbf{s}} \{\mathbf{Y}[(\nu-1)\mathbf{s}+i] - \mathbf{y}_\nu(i)\}^2 \tag{5}$$

for each segment ν, $\nu = 1, \, 2, \, 3, \, \ldots, \, N_\mathbf{s}$ and

$$\mathbb{F}^2(\nu, \, \mathbf{s}) \equiv \frac{1}{\mathbf{s}} \sum_{i=1}^{\mathbf{s}} \{\mathbf{Y}[(N-(\nu-N_\mathbf{s})\mathbf{s}+i] - \mathbf{y}_\nu(i)\}^2 \tag{6}$$

for $\nu = N_\mathbf{s} + 1, \, \ldots, \, 2N_\mathbf{s}$, where $\mathbf{y}_\nu(i)$ segment ν has been the fitting polynomial in segment ν.

- To obtain the qth order fluctuation function $\mathbb{F}_q(\mathbf{s})$, all the segments have been averaged:

$$\mathbb{F}q(\mathbf{s}) \equiv \left\{ \frac{1}{2N\mathbf{s}} \sum_{\nu=1}^{2N_\mathbf{s}} [\mathbb{F}^2(\nu, \, \mathbf{s})]^{\frac{q}{2}} \right\}^{\frac{1}{q}}, \tag{7}$$

where q has been able to take any real value except zero.

- $\mathbb{F}_\mathbf{s}$ has depended on the time scale $\mathbf{s}$ for different values of q, increasing as the scale $\mathbf{s}$ has increased.
- The scaling behavior of the fluctuation function has been determined by analyzing $log - log$ plots of $\mathbb{F}_q(\mathbf{s})$ versus $\mathbf{s}$ for each value of q. For multifractal time series, $\mathbb{F}_q(\mathbf{s})$ has increased (for large values of $\mathbf{s}$) as a power law:

$$\mathbb{F}_q(\mathbf{s}) \sim \mathbf{s}^{H(q)} \tag{8}$$

with the generalized Hurst exponent $H(q)$ depending on q. For stationary time series, the exponent $H(2)$ has been identical to the Hurst exponent.

- For monofractal time series, which have been characterized by a single exponent over all scales, $H(q)$ has been independent of q, whereas for multifractal time series, $H(q)$ has varied with q. This dependence has been considered a characteristic property of the multifractal process.

• If $q = 0$ in align (7), it has become a diverging exponent, the value of $H(0)$, which has represented the limit of $H(q)$ as q has approached zero, cannot have been determined using the standard averaging method. Therefore, researchers have used a logarithmic averaging method, given by:

$$\mathbb{F}_0(\mathbf{s}) \equiv exp\left\{\frac{1}{4N_\mathbf{s}} \sum_{v=1}^{2N_\mathbf{s}} In[\mathbb{F}^2(v, \mathbf{s})]\right\} \sim \mathbf{s}^{H(0)}, \tag{9}$$

• Note that $H(0)$ cannot be defined for time series with fractal support, where $H(q)$ diverges as $q \to 0$.

• For monofractal time series with compact support, $H(q)$ has not depended on q because the variances $\mathbb{F}^2(v, \mathbf{s})$ have been consistent across all segments. In this case, the standard averaging method has produced the same scaling behavior for all q values.

• A noticeable dependence of $H(q)$ on q has occurred when small and large fluctuations have scaled differently. For positive q, segments with large variance $\mathbb{F}^2(v, \mathbf{s})$ have dominated the average $\mathbb{F}^2(\mathbf{s})$, so $H(q)$ has described the scaling of segments with large fluctuations. For negative q, segments with small variance $\mathbb{F}^2(v, \mathbf{s})$ have been more influential in the average $\mathbb{F}^2(\mathbf{s})$, so $H(q)$ has described the scaling of segments with small fluctuations.

• In continuation with the above, the multifractal spectrum has been obtained using the relationship:

$$\tau_q = qH(q) - 1 \tag{10}$$

• An alternative measure to analyze the multifractal characteristics of a series has been to calculate the singularity spectrum, also called the multifractal spectrum $f(\alpha)$. The multifractal spectrum may have been related to τ_q through the Legendre transform:

$$\alpha(q) = \frac{d\tau_q}{dq} \tag{11}$$

and

$$f(\alpha(q)) = q(\alpha(q)) - \tau_q, \tag{12}$$

where $\alpha(q)$ has been the singularity strength or Hölder exponent, and $f(\alpha(q))$ has denoted the singularity dimension of the subset of the series that has been characterized by $\alpha(q)$.

• By employing align (10), a relationship between α and $f(\alpha)$ with $H(q)$ has been derived. It has been:

$$\alpha(q) = H(q) + qH'(q) \tag{13}$$

and

$$f(\alpha(q)) = q[\alpha(q) - H(q)] + 1, \tag{14}$$

where $H'(q)$ has been the derivative of $H(q)$.

• The strength of the multifractality has been derived from the width of the spectrum. The width of the multifractal spectrum has been calculated as:

$$width(w) = \alpha(maximum) - \alpha(minimum)$$

From MFDFA, the researchers have obtained the following exponents: q-order generalized Hurst exponents $H(q)$, q-order mass exponents (τ_q), q-order singularity exponents $\alpha(q)$, and q-order singularity dimensions $f(\alpha(q))$. The generalized Hurst exponents characterize a time series of long-term memory or persistence. The value of $H(q)$ has been calculated often for different orders of q to capture the scaling behavior of fluctuations across different scales. The $H(q)$ values obtained from MFDFA may exceed one. The value of $H(q) < 0.5$ indicates short-term reversals, negative correlation, or anti-persistence; if it equals 0.5, it suggests no correlation or a random walk with no memory. The $H(q) > 0.5$ indicates long-term correlation or positive persistence.

The mass exponent (τ_q), also known as the moment exponent, characterizes the distribution of fluctuations at different scales. It has provided information about how the moments of the probability distribution function of fluctuations scale with the order of the moment q. The singularity exponents $\alpha(q)$ have characterized the local regularity or irregularity in the data. It has been obtained from the multifractal spectrum and describes how the singularity strength varies with scale. The singularity dimension $f(\alpha(q))$, also known as the multifractal spectrum, has described the distribution of singularity strengths across different scales. It has provided a comprehensive view of the multifractal properties of the dataset. The multifractal of the dataset has been measured by the width of the multifractal spectrum, which has been represented by the difference between the maximum value of $\alpha(q)$ and the minimum value of $\alpha(q)$. Matlab software has been used to find the MFDFA, and the coding has been taken from the articles [45, 46].

The asymmetry of the MFDFA spectrum has provided insights into the distribution of singularities in a time series. It has indicated whether large fluctuations or small fluctuations dominate the multifractal behavior. A left-skewed spectrum has suggested the dominance of small fluctuations, while a right-skewed spectrum has indicated the prevalence of large fluctuations. This characteristic has been widely used to identify and interpret the nature of variability and scaling in complex systems, including climate and environmental data. The asymmetry measure has offered a deeper understanding of the imbalance in multifractal structures, enhancing the analysis of non-linear and non-stationary data.

2.4 *Correlation coefficient*

A statistical measure of the degree to which two variables have shown a linear relationship is the correlation coefficient. Correlation analysis has allowed researchers to investigate whether changes in one variable have correlated with changes in another. After data collection, the scatter plot is used to visualize the data, with one variable drawn along the x-axis and another variable plotted along the y-axis. Researchers have been able to examine the scatter plot through their sight to determine whether there are any observable patterns or whether the variables have a linear connection. It is implied that a straight line could plausibly match the data points in a linear connection.

The correlation coefficient has been constrained to a range from -1 to 1. The values within this range have indicated the strength and direction of the correlation. Specifically, a correlation coefficient falling between -1 and 0 has signified a negative correlation, while a value of 0 has suggested no correlation at all. On the other hand, coefficients ranging from 0 to 1 have indicated a positive correlation. In instances where the coefficient has precisely equaled -1 or 1, it has denoted a perfect negative or perfect positive correlation, respectively. The positive coefficients have signified that the variables have changed in the same direction, whereas a negative coefficient has implied they have varied inversely. The magnitude of the correlation coefficient, irrespective of its sign, has been represented by its absolute value. The correlation coefficient values have quantified the strength of the correlation coefficient. When the correlation value has reached 1 (either positively or negatively), the variables have a strong correlation between them [47, 48]. For this analysis, Excel software has been used.

3. Data description

To analyze stratospheric ozone depletion's impact on climate variables such as temperature and precipitation, this study has used monthly data ranging from 1979 to 2023. The Global Monthly Temperature Anomaly (GMTA), Global Monthly Precipitation Anomaly (GMPA), and Southern Hemisphere Minimum Ozone (SHMO$_3$) data have been extracted from the data reservoirs 'Our World in Data' [49], 'Copernicus Climate Data' [50], and 'NASA Climate Data' [51], respectively. GMTA data has been drawn directly from the data reservoir 'Our World Data' as monthly data. The combined land-surface air and sea-surface water temperature anomaly has been given as the deviation from the 1951 to 1980 mean. The temperature data has been given in Celsius units. SHMO$_3$ data has also been obtained directly from the source 'NASA Climate Data' as monthly data for the Southern Hemisphere, with a few missing data points. The missing data have been adjusted by the average of the preceding and succeeding two years of its respective monthly data. It has been measured in units of Dobson (DU). The total precipitation data have also been available as a monthly data source for the various locations of the world under the division of "Essential Climate Variables for the Assessment of Climate Variability Since 1979 to the Present".
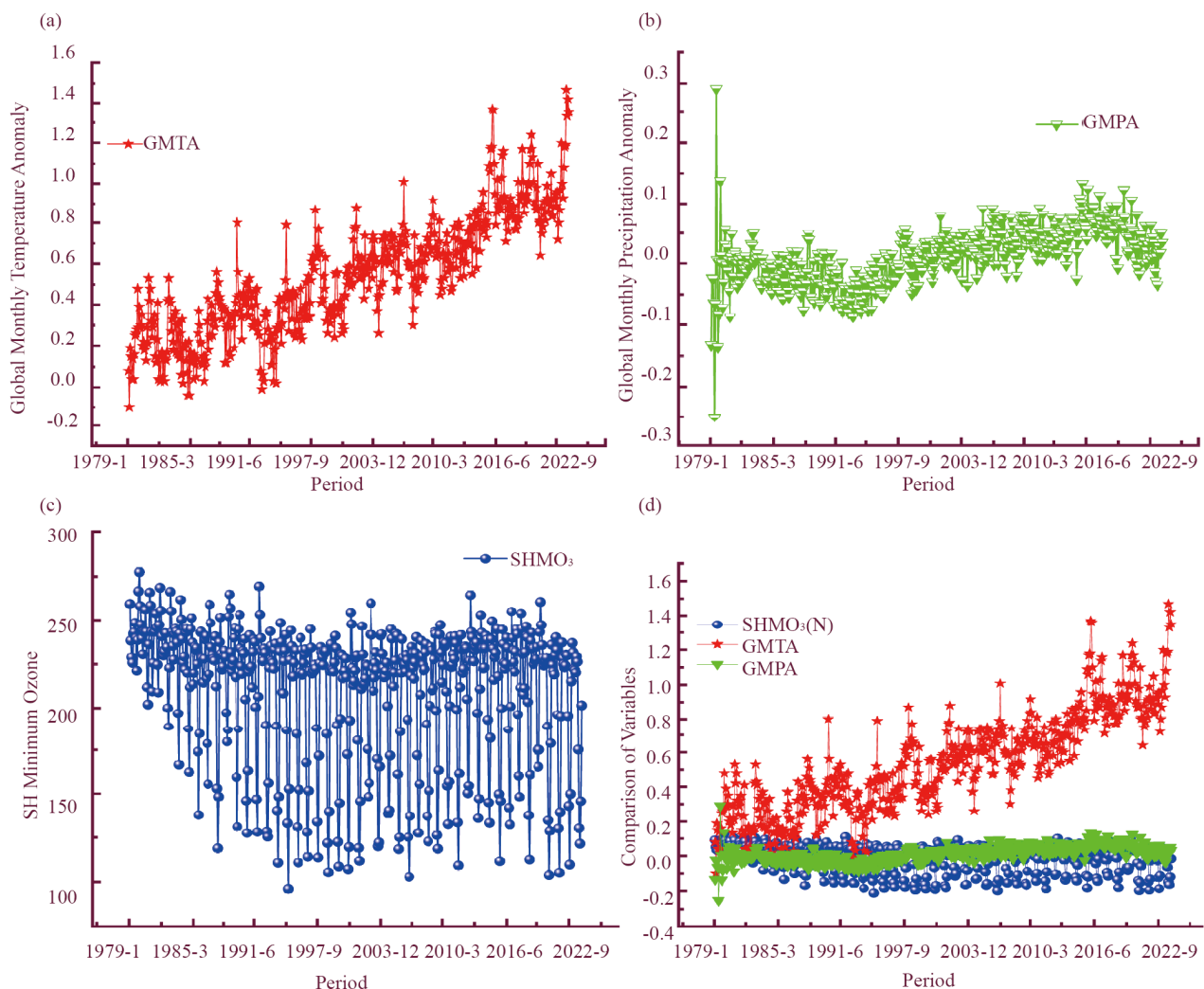

Figure 3. Visualization of variables: (a) GMTA, (b) GMPA, (c) SHMO$_3$, and (d) comparison of GMTA and GMPA with normalized SHMO$_3$

The average of the total precipitation at all locations in the data reservoir has been considered as GMPA. Precipitation is defined as the accumulation of liquid and frozen water (including rain and snow) that falls to the surface of the earth. Precipitation variables have excluded fog, dew, and the precipitation that evaporates in the atmosphere before reaching the surface. The monthly mean precipitation data has been presented in units of meter 'm', meaning that the amount of precipitation that falls over a day has been expressed as "m/day". For ease of reference, the data has been converted to mm/day by multiplying it by $1,000$. Figure 3 is a graphical representation of the variables GMTA, GMPA, and SHMO$_3$ in Figures 3(a), 3(b), and 3(c), respectively. SHMO$_3$ data has been normalized by using the statistical method $(x - \bar{x})/N$ to compare it with other variables, which is displayed in Figure 3(d).

4. Results and discussion

In this section, the analysis has found the fractal dimension of three variables: SHMO$_3$, GMTA, and GMPA, using Excel software. The fractal dimension values of the variables have been obtained from the Hurst exponent values by using the method of rescaled range analysis.
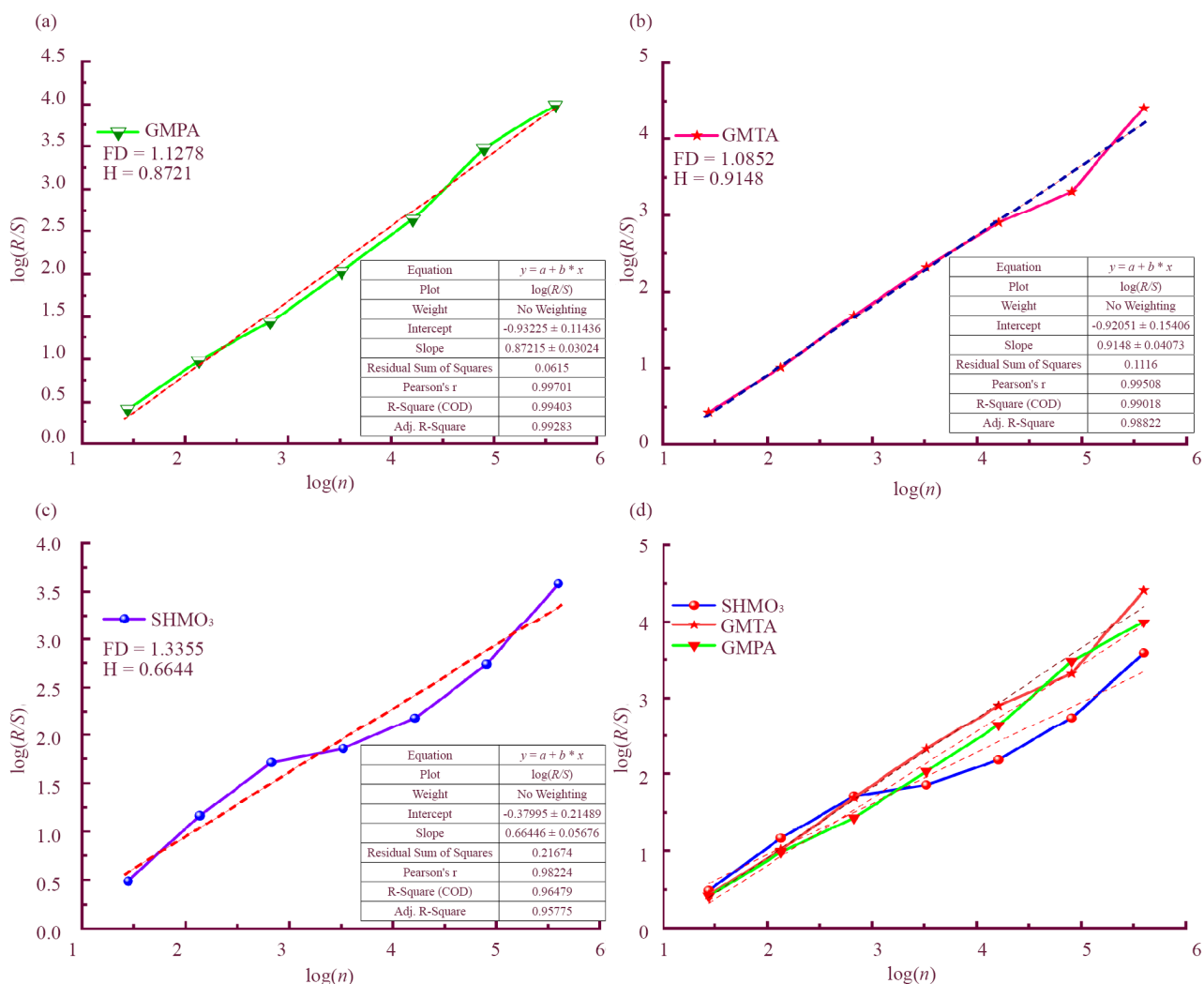

Figure 4. The $log - log$ plot of (a) GMPA, (b) GMTA, (c) SHMO$_3$, and (d) a combination of all the variables in a single plot

Each variable consists of 540 time-series data points, which have been divided into 7 segments as 2, 4, 8, 16, 32, 64, and 128 in the powers of 2. The x-axis values of the plot have represented the logarithm of these segment sizes (n), while the corresponding y-axis values have represented the logarithm of the average rescaled range values. Each point on the plot has been represented by the segment size. Figure 4 depicts the $log - log$ plots of GMPA, GMTA, SHMO$_3$, and the combination of all three variables. In Figure 4(a), the light green curve has been indicated as the regression curve of GMPA, with its corresponding linear fit being represented by red dashed lines. Next to it, in Figure 4(b), the non-linear the red curve has been represented as the regression curve of GMTA, while the small blue dashed lines have depicted its linear fit. In Figure 4(c), the blue curve has been represented by SHMO$_3$, and its linear fit has been denoted by red dashed lines. Ultimately, Figure 4(d), shows the comparison of $log - log$ plots of all variables. All plots have exhibited a non-linear relationship. To estimate the Hurst exponent values, linear regression has been applied to the curves. The slope of the linear fit is represented as the Hurst exponent (H). The obtained and calculated H & FD values have been mentioned in their respective graphs. Remarkably, all regression curves have lain above the linear fit line, indicating persistence in the data. Among the variables, GMTA has had the highest Hurst exponent, suggesting the strongest persistence and most predictable trends, followed by GMPA and SHMO$_3$. This has indicated that GMTA's behavior over time has been influenced by strong long-term memory effects, which could have had implications for climate modeling and prediction. They have had a chance of a reduction in the data value after a few months. Therefore, the variables GMTA, GMPA, and SHMO$_3$ has exhibited persistence with long-range memory. From the result, it has been observed that SHMO$_3$ has more roughness and complexity, which has been followed by GMPA and GMTA.

The obtained values of the Hurst exponent (H) and fractal dimension (FD) have been displayed in Table 1. Table 1, has shown the value of the fractal dimension (FD) of SHMO$_3$, as 1.3355. This value has indicated a higher level of complexity, irregularity, and less level of persistence over time. It has suggested a significant degree of persistence or long-range dependence on the data, with trends or patterns that have tended to recur on different timescales contributing to its fractal dimension. The FD value of GMTA has been 1.0852, indicating that the variable has a medium level of complexity and irregularity compared to SHMO$_3$. It has been suggested a relatively smooth, regular, and highly persistent behavior over time. The data have exhibited some degree of randomness or short-range dependence, with more recurring patterns on different timescales. For GMPA, the fractal dimension value is around 1.127, which indicates that the data has moderate complexity with some recurring patterns or structures across different scales. It's not entirely smooth (like a straight line) but also not highly irregular (like random noise). The value suggests a degree of long-range dependence or moderate persistence in the data, where trends or features may have persisted over time or across different resolutions. This table has summarized the key quantitative findings from the analysis of the three variables-SHMO, GMTA, and GMPA.

**Table 1.** The Hurst exponent (H) and Fractal dimension (FD) values of the variables

Variables	H	FD
SHMO$_3$	0.6644	1.3355
GMTA	0.9148	1.0852
GMPA	0.8721	1.1278

The results of this study have demonstrated that all analyzed time series exhibit fractal characteristics and long-range persistence. Therefore, multifractal analysis, specifically the MFDFA procedure, has been employed to measure this fractal behavior.

Next to this, the study discussed the outcomes of the variables from the MFDFA procedure using MATLAB software. The procedure has analyzed 45 years of monthly data, spanning from 1979 to 2023, which has a time series of 540 data points. The segment sizes 's' were selected logarithmically between a minimum of 4 and a maximum of 540, with 8 equally spaced resolutions to ensure adequate coverage of both short and long timescales. A total of 25 'q' values were used, ranging symmetrically from -5 to 5, to explore multifractality across a spectrum of small and large fluctuations. A

least squares method was applied for polynomial fitting, with the detrending performed using a first-order polynomial to effectively remove linear trends within each segment.

Figure 5 has shown *log-log* plots that represent the scale**s** versus fluctuation function $F_q(\mathbf{s})$ for different q-values obtained from the MFDFA. These plots have allowed us to explore the scaling behavior of each variable in Figure 5(a) $SHMO_3$, Figure 5(b) GMTA, and Figure 5(c) GMPA. The approximate linearity of the plots across different q-values has indicated the presence of a scaling relationship. For positive q-values, the fluctuation function $F_q(\mathbf{s})$ has emphasized larger fluctuations, while for negative q-values it has emphasized smaller fluctuations. The difference in slopes across q-values has reflected the multifractal nature of the data. GMPA, in Figure 5(c), has exhibited consistent scaling across different scales **s**. The spread of $F_q(\mathbf{s})$ for varying q-values has suggested moderate multifractal characteristics which has observe from the more negative values of q. Similar to GMPA but with a slightly more pronounced separation between q-values, GMTA in Figure 5(b) has indicated stronger multifractality or a broader range of fluctuation dynamics. $SHMO_3$, in Figure 5(a), has displayed a steeper increase in $F_q(\mathbf{s})$, particularly for higher q-values. This has suggested that larger fluctuations have dominated the scaling behavior and that the multifractality may have been influenced more strongly by extreme values. Each variable has exhibited unique scaling behaviors, as reflected in the $F_q(\mathbf{s})$ plots. These differences have been tied to their multifractal properties and have been quantified by the generalized Hurst exponent, mass exponent, and singularity spectrum. $SHMO_3$ has likely had the strongest multifractality, followed by GMTA and GMPA. This scaling behavior has indeed shaped the MFDFA spectrum $f(\alpha)$.
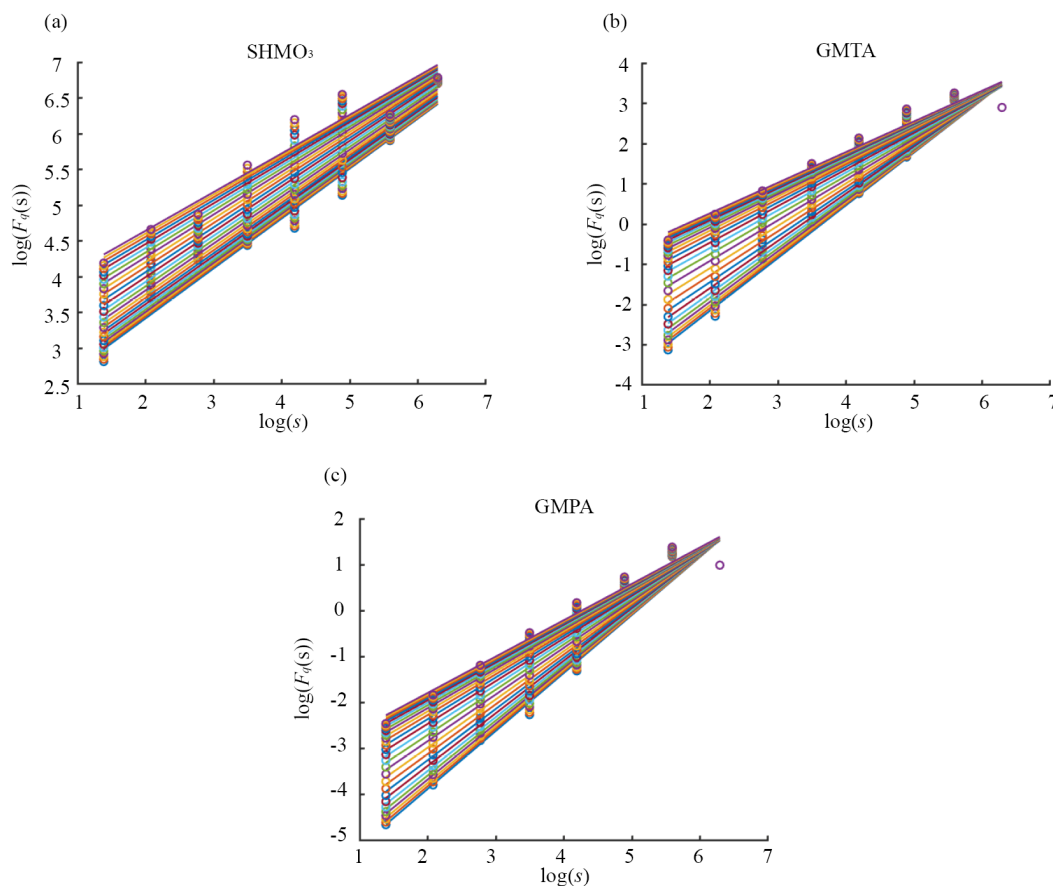
Figure 5. The *log-log* plot of sclae **s** versus function $F_q(\mathbf{s})$ for the variables (a) $SHMO_3$, (b) GMTA, and (c) GMPA with different q-values along with their linear fits

The obtained generalized Hurst exponent $H(q)$ values for different q-values have varied between 1.0547 to 0.6363 for SHMO$_3$, 1.4202 to 1.1213 for GMTA, and 1.3332 to 0.8323 for GMPA. In comparison, the generalized Hurst exponent values of GMTA have been observed to be higher than the other variables. Throughout all q-values, the generalized Hurst exponents have remained above 0.5 for all the variables, indicating long-range dependence, especially GMTA values of all q-order have exceeded 1, which means strong range dependence and persistence. The variability of the generalized Hurst exponents across different scales has offered insights into the multifractal characteristics of the time series, showcasing varying degrees of long-term memory at different scales. Particularly, the GMTA values have consistently exhibited higher levels than the others, which can be visualized in Figure 6(a). The $H(q)$ values of all the variables have lied between 0.6 and 1.4202, implying that all are persistent. The maximum value of SHMO$_3$ has been found to be lower than the minimum values of GMTA. Although GMTA and GMPA have both demonstrated persistence, there have been distinctions in their specific dynamics and suggested variations in the underlying processes. GMPA has exhibited persistence to a slightly lesser extent or with different dynamics compared to GMTA.
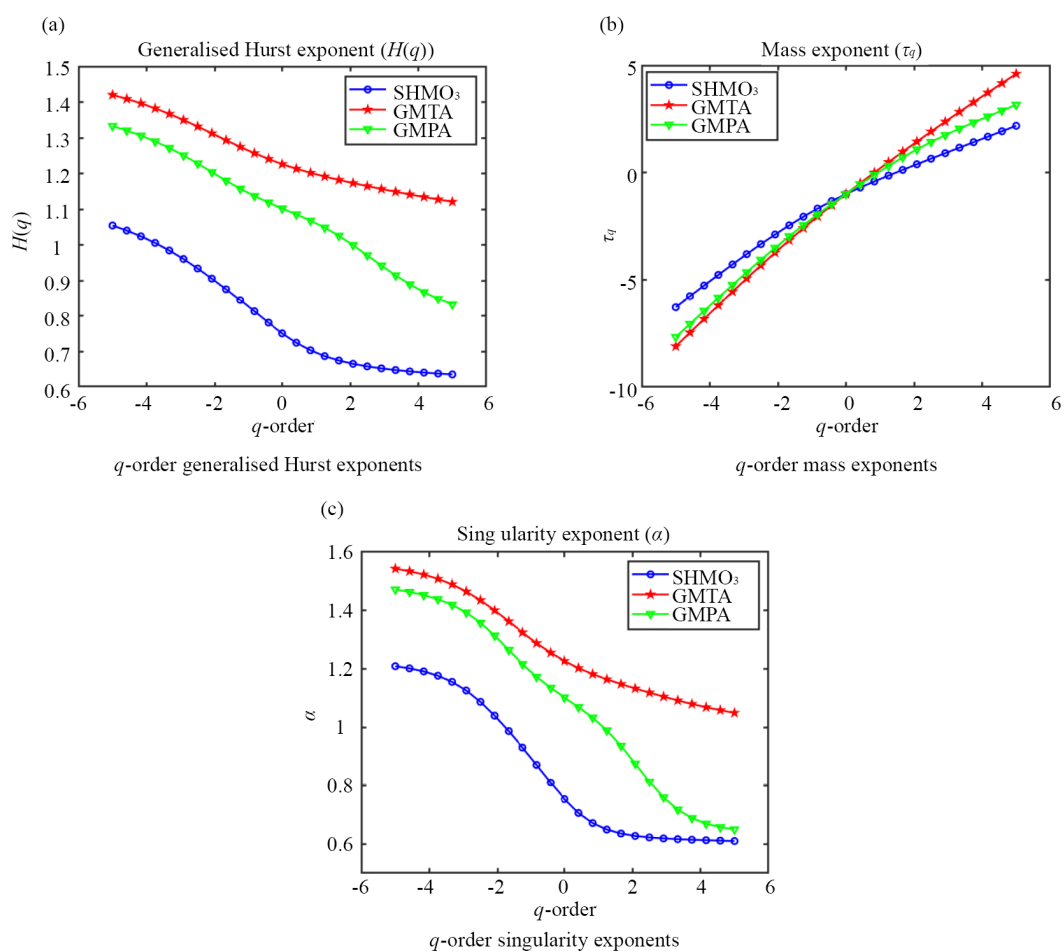

Figure 6. The exponents value from MFDFA method

The mass exponents (τ_q) values of the variables have exhibited a range of variation across different q values, which are from -6.2737 to 2.1816 for SHMO$_3$, -8.101 to 4.6064 for GMTA, and -7.6658 to 3.162 for GMPA. In multifractal analysis, the τ_q parameter has been associated with the generalized Hurst exponents and described how the fluctuation function has scaled for a given q-order. Positive τ_q values have signified areas of high singularity strength, indicating pronounced fluctuations or irregularities in the time series. Conversely, negative τ_q values have indicated regions of low

singularity strength, suggesting smoother or more regular segments within the series. By comparing the τ_q values of three distinct variables, researchers have assessed how the distributions of singularity strength differ among them. Notably, the τ_q values have increased with higher q values, indicating multifractality within the data.

These τ_q values have complemented the singularity exponents $\alpha(q)$ and singularity dimensions $f(\alpha(q))$ values by offering insights into the distribution of singularity strengths across various scales. Analyzing τ_q values has enabled the study to discern relationships between variables by comparing their singularity strength distributions and characterizing their multifractal properties. The Figure 6(b), has been displayed the mass exponents (τ_q). SHMO$_3$, GMTA, and GMPA have been depicted in blue, red, and green colors, respectively. The graph has illustrated the q-order on the x-axis ranging from -5 to 5, while the mass exponent values have ranged from -10 to 5 on the y-axis. The GMTA values, which have spanned from a low of -8.1 to a high of 4.6063, have shown greater variability than the other variables. The graph of SHMO$_3$ has shown a non-linear curve, which has indicated more multifractality. All three variables have exhibited non-linear graphs, which have indicated the presence of multifractality.
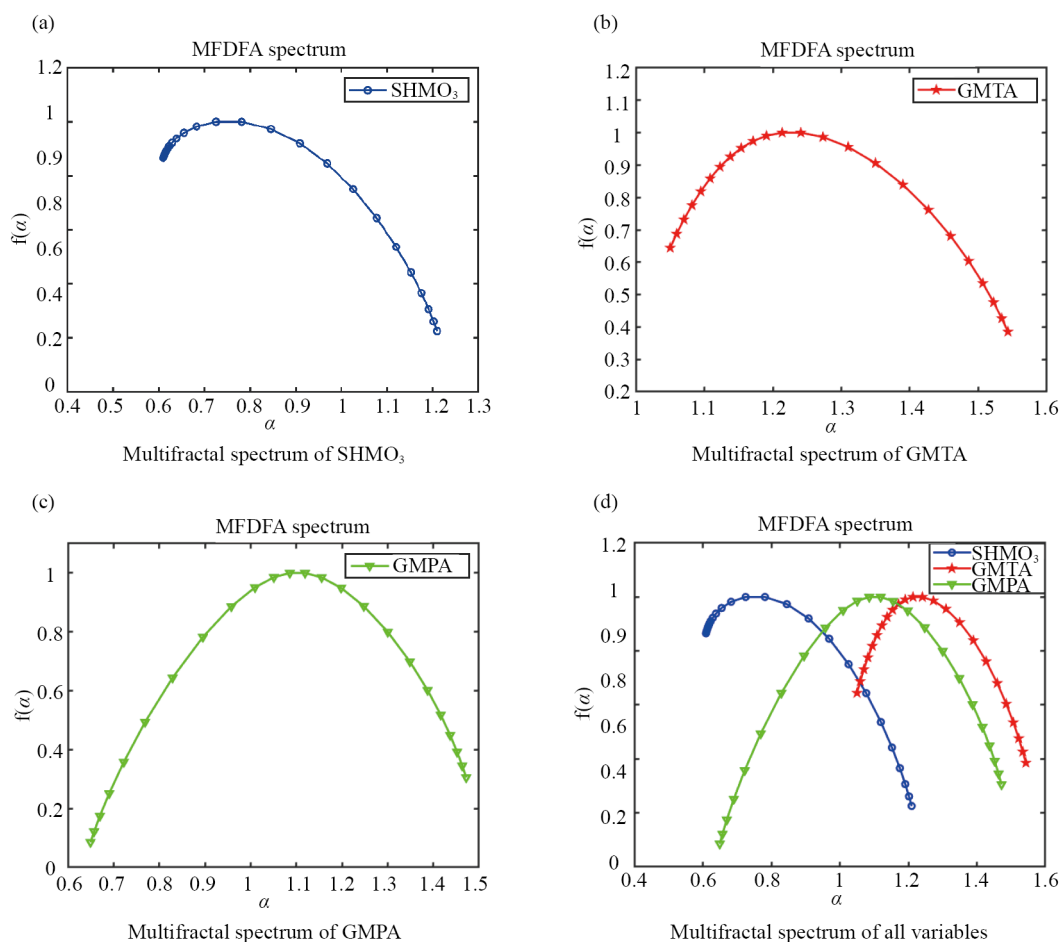

Figure 7. MFDFA spectrum

The singularity exponent values of the variables, across various q values, have ranged from 1.2096 to 0.6095 for SHMO$_3$, 1.5431 to 1.0502 for GMTA, and 1.4721 to 0.6495 for GMPA. These values have characterized the local regularity or irregularity within the data. The $\alpha(q)$ values of all variables have fallen between 0.6 and 1.54. A $\alpha(q)$ value close to 1 suggested strong singularities or points of non-analytic behavior in the time series, often corresponding to regions of extreme fluctuations or irregularities. A $\alpha(q)$ value greater than 1 has indicated a smoother curve than expected,

while a value less than 1 has suggested more roughness. All the values of GMTA lie above one. Significant variations in the singularity exponents across scales have suggested multifractality, indicating different degrees of irregularity or roughness at different scales. Positive $\alpha(q)$ values have indicated regions of higher irregularity, reflecting varying degrees of irregularity across the series. Figure 6(c) shows the singularity exponent's graph. This study has observed from these graphs that the values of GMTA (the red color line) are higher than other variables, and all the values are above one. They have a greater local inconsistency in the SHMO$_3$ results.

The multifractal spectrum has provided valuable insights into the extent of multifractality exhibited by the time series data. The width of this spectrum has served as a key indicator of the system's multifractal complexity. A wider spectrum means a more multifractal nature, which has indicated greater complexity within the time series. The multifractal spectrum has been drawn as a plot of $\alpha(q)$ versus $f(\alpha(q))$, in Figure 7. In Figure 7(a), the spectrum of SHMO$_3$ has exhibited a wider width, indicating increased complexity and roughness across different scales. The left asymmetry observed in the SHMO$_3$ spectrum has been indicating that the time series has been exhibiting more large fluctuations, which should be examined using positive values of q. Figure 7(b) displays the narrow spectrum of GMTA and its left asymmetry observed has been suggesting that the time series has also been showing larger fluctuations, which can be best observed with the help of positive values of q. Figure 7(c) presents the spectrum of GMPA, which also demonstrated a wider width compared to GMTA and SHMO$_3$ and its right asymmetry observed has been indicating the presence of more small fluctuations in the time series, which should be analyzed using negative values of q. Therefore, SHMO$_3$ and GMPA have exhibited higher multifractality and roughness across different scales. Figure 7(d) visualizes the multifractal spectrum of all variables, enabling easy identification of spectrum width.

In Table 2, $\alpha(q)$ maximum ($\alpha(q)$ max), $\alpha(q)$ minimum ($\alpha(q)$ min) value, and the width (ω) of the multifractal spectrum have been exhibited, with GMPA (0.8278) being shown as the widest spectrum, followed by SHMO$_3$ (0.6037), and then GMTA (0.4991). Generally, a broader spectrum has suggested higher multifractality or complexity across various scales. The spectrum width has reflected the complexity of the scaling behavior. The data in this table have highlighted that GMPA has exhibited the most multifractality, while GMTA has shown the least multifractality among the variables, which has helped to predict the variable in the future. These characteristics have underscored the interconnected and complex nature of these variables in climate change studies. The spectrum width has reflected the complexity of the scaling behavior. The data in this table have highlighted that GMPA has exhibited the most multifractality, while GMTA has shown the least multifractality among the variables, which has helped to predict the variable in the future. These characteristics have underscored the interconnected and complex nature of these variables in climate change studies. Irregularities across different scales have been evident in all variable's time series data. GMPA has exhibited the highest level of multifractality, suggesting a more complex and heterogeneous scaling structure. SHMO$_3$ has shown moderate multifractality, while GMTA has had the least, implying relatively homogeneous scaling behavior. A wider spectrum has suggested that the variable has been influenced by multiple processes operating at different scales, which has been crucial for understanding the variability and complexity of climate systems.

Table 2. The maximum and minimum values of the singularity exponents value $\alpha(q)$, and spectrum width (ω) of the variables SHMO$_3$, GMTA, and GMPA

Variables	$\alpha(q)$ max	$\alpha(q)$ min	ω
SHMO$_3$	1.2126	0.6089	0.6037
GMTA	1.5460	1.0469	0.4991
GMPA	1.4750	0.6472	0.8278

The correlation coefficient has been applied to the exponent values of $H(q)$, τ_q, $\alpha(q)$, derived from MFDFA for each variable, and the actual variable data values from the data repository. This study has used the correlation values between the variables generated from Excel software. Table 3 gives the obtained values of the correlation coefficient between the variables. The correlation coefficients of the q-order generalized Hurst exponents value $H(q)$, for the variables

SHMO$_3$, GMPA, and GMTA have a positive and strong correlation between them (0.9571 and 0.9952). The graph 8(a) has illustrated this concept, with the abscissa values representing the $H(q)$ value of SHMO$_3$ and with the ordinates representing GMTA and GMPA. Figure 8's color depiction of GMTA and GMPA has been red and green, respectively.

The correlation coefficients between SHMO$_3$, GMPA, and GMTA for the q-order mass exponent values (τ_q) have been obtained as 0.9994 and 0.9972, respectively. The exponents have correlated strongly and positively with one another. Figure 8(b) has an illustrated correlation coefficient plot of the mass exponent values (τ_q) of the variables, whose abscissa and ordinate are the τ_q values of SHMO$_3$ and the τ_q value of GMPA and GMTA. Positive strength has been shown by the correlation coefficient values of $\alpha(q)$ between the pairings of SHMO$_3$ with GMTA and GMPA, which have been 0.9910 and 0.9465, respectively. The correlation graph of the $\alpha(q)$ has been displayed in Figure 8(c). In this case, the x-axis has reflected the $\alpha(q)$ values of SHMO$_3$, and the corresponding y-axis has displayed the $\alpha(q)$ values of GMTA and GMPA. Both the data values have traveled in the same positive direction. The correlation coefficients of the actual data values of the variables have been found to have an extremely poor negative correlation.
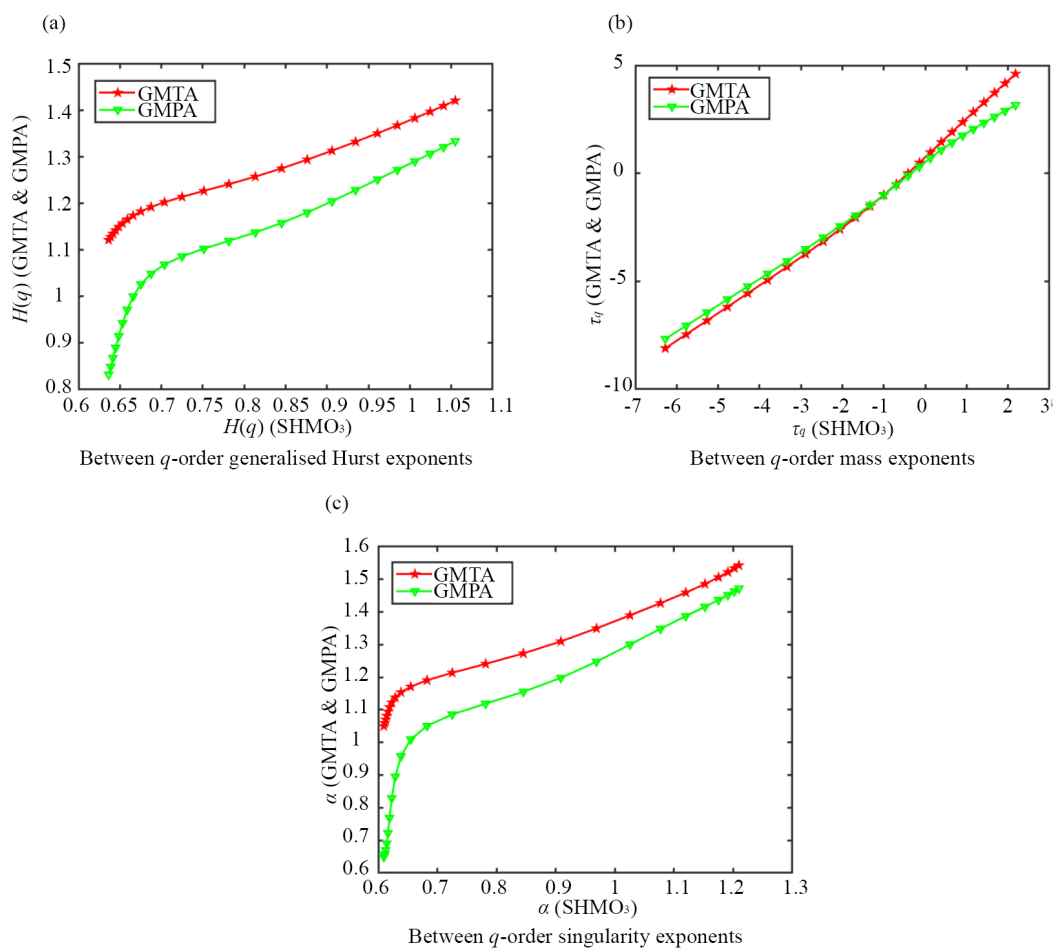
Figure 8. Comparison of correlation coefficients between the variables SHMO$_3$, GMTA, and GMPA from MFDFA exponent values

The direction and magnitude of correlations have been observed through the high positive correlation coefficients between the exponent values $H(q)$, τ_q, $\alpha(q)$ for SHMO$_3$, GMPA, and GMTA, indicating a strong interdependence among the variables. Specifically, the generalized Hurst exponent $H(q)$ has shown correlations of 0.9571 (SHMO$_3$-GMPA) and 0.9952 (SHMO$_3$-GMTA). This has implied that the scaling properties of these variables have aligned closely, reflecting similar multifractal behaviors. The mass exponent τ_q has exhibited even stronger correlations (0.9994 and 0.9972),

emphasizing that the cumulative scaling behavior of these variables has been nearly identical. The singularity strength $\alpha(q)$ has shown slightly lower but still significant correlation values of 0.9910 and 0.9465, which has suggested that the multifractal spectrum widths have been strongly related across these variables. The correlation coefficients of the actual data values have been negatively correlated, indicating that direct comparisons of raw data trends might not have fully captured the underlying interdependencies revealed by the multifractal analysis.

The mechanisms behind these relationships have likely arisen from the interdependent dynamics of climate variables. $SHMO_3$ has directly affected atmospheric processes, such as the radiation balance and chemical composition, which, in turn, have influenced GMTA and GMPA. For instance, the depletion of ozone has led to increased ultraviolet (UV) radiation, impacting atmospheric circulation patterns, which have influenced temperature anomalies and precipitation distributions. The strong correlations in the multifractal exponents have suggested that these effects have not been isolated but are part of a coupled system with shared scaling properties and long-term memory. While the high correlations have indicated strong relationships, they have not implied direct causality. The observed correlations may have been mediated by external factors such as seasonal variations, solar radiation, or aerosol concentrations that have affected all three variables simultaneously. Seasonal cycles and regional climate phenomena, such as El Niño-Southern Oscillation (ENSO), may have introduced periodic trends that have amplified or suppressed these correlations. The negative correlation in raw data values may have reflected phase differences or offsets in how each variable has responded to external drivers, which multifractal analysis has helped to disentangle. These have been the implications for causality and external factors.

Finally, from the results, MFDFA exponent values have been most useful in determining the irregularity, robustness, and persistence of the variable and exponents form it has used to find the relationship between the variables. This usefulness has been highlighted through the comparison of the correlation coefficient findings between the values acquired from the real data and the MFDFA exponent values. Therefore, based on the results, the study has concluded that ozone depletion influences climate change variables (GMPA & GMTA). It has been shown that the MFDFA approach facilitates a thorough examination of the variables; on the other hand, the study got the information that real data alone is not enough for the analysis to find the relationship between them.

Table 3. Correlation coefficient values comparison between the variables GMTA, and GMPA with the $SHMO_3$ for the MFDFA exponent values and real data

| Exponents | Variables | Correlation coefficients | |
		GMPA	GMTA
$H(q)$	$SHMO_3$	0.9571	0.9952
τ_q	$SHMO_3$	0.9994	0.9972
$\alpha(q)$	$SHMO_3$	0.9465	0.9910
Data	$SHMO_3$	-0.0834	-0.1236

5. Limitations of the study

This study has some limitations that warrant attention: Missing data for the three variables-5.9% ($SHMO_3$), 0.5% (GMPA), and 0.1% (GMTA)-was imputed using the classical monthly mean method. While this approach produced results consistent with the raw data, it may overlook short-term trends and fluctuations, potentially introducing biases. Advanced imputation techniques, such as regression models or machine learning approaches, could address these issues in future studies. The analysis focused on three variables derived from a single dataset over a limited temporal scale. While the results highlight significant multifractal properties and correlations among these variables, their applicability to other climate variables or regional contexts is limited. Future research should incorporate broader datasets with additional climate variables and extended spatial-temporal coverage.

The methods employed, including Fractal Dimension analysis, Multifractal Detrended Fluctuation Analysis (MFDFA), and correlation coefficient analysis, effectively reveal the nonlinear dynamics and long-range correlations among variables.

However, they do not fully capture external drivers or causality in climate ozone interactions. Integrating additional methods, such as causal inference techniques, wavelet coherence analysis, or advanced machine learning models, could provide a more comprehensive understanding of these complex systems. The observed correlations (e.g., Generalized Hurst Exponent: 0.9571 and 0.9952; Mass Exponent: 0.9994 and 0.9972) indicate strong interdependence among the variables. However, they may also reflect external factors, such as seasonal variations or shared atmospheric drivers, rather than direct interactions. The negative correlations in raw data values (-0.083 and -0.1236) suggest possible temporal misalignment, which should be explored further using multivariate models. By addressing these limitations, future studies can build on the findings of this research and contribute to a deeper understanding of climate-ozone dynamics. The discrepancy between scaling behavior in $F_q(\mathbf{s})$ plots and the width of singularity spectra has highlighted the inherent complexity of multifractal analysis. The dominance of larger or smaller fluctuations has potentially skewed interpretations of multifractality when spectrum asymmetry and width have not been jointly considered. Future studies are encouraged to incorporate additional metrics to better disentangle the respective contributions of fluctuation intensity and diversity to multifractal behavior. Techniques such as MF-DXA [52], MF-X-DFA [53], and MFCCA [54] have been proposed to enhance the identification and quantification of multifractal behaviors in cross-correlations, addressing the limitations of existing methods. These methods will be utilized in our future work.

6. Conclusion

Based on the acquired findings, this study has suggested that multifractality is a powerful measure for determining fractal behavior in dynamic systems. The MFDFA model has also been a reliable tool for identifying multifractal behavior. This approach has used climate change variables, such as GMTA and GMPA, to determine their relationship with ozone depletion. From the results, it has been clearly proven that all the variables are fractal and exhibit multifractal behavior. From the derived exponent values, it has been observed that there is a high correlation between ozone depletion and climatic factors. All the variables have demonstrated multifractal properties, measured by the width of the multifractal spectrum. GMTA has shown less multifractality than $SHMO_3$, which, in turn, has been followed by GMPA. The values of the Hurst exponent have highlighted the complexity and irregularity of the variables. It has been observed that GMTA and GMPA exhibit a high level of persistence, whereas $SHMO_3$ has a lower persistence level. The analysis has revealed distinct multifractal characteristics for each variable. $SHMO_3$ and GMTA have exhibited stronger scaling behaviors for larger fluctuations, as reflected in their $F_q(\mathbf{s})$ plots and the right asymmetry of their singularity spectra. In contrast, GMPA, characterized by left asymmetry signifying dominance by smaller fluctuations, has demonstrated greater overall multifractality due to its wider singularity spectrum. These findings have underscored the complementary interplay between scaling behavior and spectrum width in multifractal analysis. While $SHMO_3$ and GMTA have highlighted the intensity of fluctuations, GMPA has emphasized the diversity of fluctuation patterns.

The results from the correlation coefficients have helped the study to find the strength and direction between the variables. Thus, the results of this study have confirmed that ozone depletion has an impact on climate change. The study has observed another reality that GMTA and GMPA have increased more since 1985 and they will be greater in the future. The rapid increment of the GMTA has occurred not only due to ozone depletion but also due to other factors. This rapid increase has not only affected people through natural calamities but may also lead to the emergence of new diseases. The high positive correlation (> 0.9) observed among the MFDFA exponents for ozone depletion, global temperature, and precipitation has demonstrated a strong interdependence among these variables. These findings have highlighted that targeted actions to mitigate ozone depletion, such as the strict enforcement of international protocols (e.g., the Montreal Protocol), has the potential to reduce cascading effects on global temperature and precipitation. The multifractal nature of these variables has emphasized the necessity for dynamic and nonlinear models to predict future climate scenarios more effectively. This approach has paved the way for the development of more accurate and region-specific climate adaptation plans.

Furthermore, practical measures, such as enhancing public awareness and supporting sustainable technologies, have been identified as key strategies to reduce anthropogenic contributions to ozone depletion and its secondary effects.

These findings have underscored the interconnectedness of atmospheric variables and have reinforced the importance of integrating them into global climate models to provide a robust foundation for informed policymaking and environmental management. Therefore, based on these results, this study recommends that governments take measures to reduce factors contributing to the increase in GMTA and to protect all life on the planet. In future studies, we plan to investigate additional factors influencing climate change using advanced techniques such as cross-MFDFA, Multivariate Hurst Exponents, bifurcation analysis, neural networks, and fractal interpolation methods. These methodologies will enable us to explore long-range correlations, nonlinear dynamics, and complex interdependencies among climate variables. Such approaches will provide deeper insights into the multifaceted nature of climate systems and help to improve predictive models for better climate change mitigation and adaptation strategies.

Acknowledgement

Conflict of interest

The authors declare that they have no conflicts of interest.

References

[1] Farman JC, Gardiner BG, Shanklin JD. Large losses of total ozone in Antarctica reveal seasonal ClO X/NO X interaction. *Nature*. 1985; 315(6016): 207-210.

[2] Dameris M. Depletion of the ozone layer in the 21st century. *Angewandte Chemie International Edition*. 2010; 49: 489-491.

[3] Jonas MO. The ozone hole and a phase change in lower stratospheric temperature. *World Journal of Advanced Research and Reviews*. 2024; 21(2): 1319-1324.

[4] Jan B, Zai MA, Afradi FK, Aziz Z. Study nonlinear dynamics of stratospheric ozone concentration at Pakistan Terrestrial region. *Journal of Atmospheric and Solar-Terrestrial Physics*. 2018; 168: 48-57.

[5] Komhyr WD, Evans RD. *Operations Handbook-Ozone Observations with a Dobson Spectrophotometer*. World Meteorological Organization Global Ozone Research and Monitoring Project; 1980.

[6] European Environment Agency. *Current State of the Ozone Layer*. Available from: https://www.eea.europa.eu/en/topics/in-depth/climate-change-mitigation-reducing-emissions/current-state-of-the-ozone-layer [Accessed 22nd November 2023].

[7] U.S. Department of State. *The Montreal Protocol on Substances That Deplete the Ozone Layer*; 2023. Available from: https://www.state.gov/key-topics-office-of-environmental-quality-and-transboundary-issues/the-montreal-protocol-on-substances-that-deplete-the-ozone-layer [Accessed 22nd November 2023].

[8] U.S.National Oceanic and Atmospheric Administration (NOAA). *Temperature Anomalies vs. Temperature*. Available from: https://www.ncei.noaa.gov/access/monitoring/dyk/anomalies-vs-temperatur [Accessed 22nd November 2023].

[9] Zhu F, Si F, Zhou H, Dou K, Zhao M, Zhang Q. Sensitivity analysis of ozone profiles retrieved from sciamachy limb radiance based on the weighted multiplicative algebraic reconstruction technique. *Remote Sensing*. 2022; 14(16): 3954.

[10] Kamalu CI, Anusi M, Uzondu F, Effiong E, Obibuenyi I, Onyelucheya O. Modeling the kinetics of ozone layer depletion using systems of ODEs. *International Journal of Renewable Energy Technology*. 2015; 4(5): 1.

[11] Misra OP, Kalra P. Effect of rising temperature due to ozone depletion on the dynamics of a prey-predator system: A mathematical model. *Applications and Applied Mathematics: An International Journal (AAM)*. 2012; 7(2): 4.

[12] Cheng CH, Huang SF, Teoh HJ. Predicting daily ozone concentration maxima using fuzzy time series based on a two-stage linguistic partition method. *Computers & Mathematics with Applications*. 2011; 62(4): 2016-2028.

[13] Hartmann DL. The Antarctic ozone hole and the pattern effect on climate sensitivity. *Proceedings of the National Academy of Sciences*. 2022; 119(35): e2207889119.

[14] Roy R, Kumar P, Kuttippurath J, Lefevre F. Chemical ozone loss and chlorine activation in the Antarctic winters of 2013-2020. *Atmospheric Chemistry and Physics*. 2024; 24(4): 2377-2386.

[15] Tuck AF, Hovde SJ. Fractal behavior of ozone, wind and temperature in the lower stratosphere. *Geophysical Research Letters*. 1999; 26(9): 1271-1274.

[16] Khan MA, Zai Y, Hussain MA, Ansari MR. Investigating chaos in ozone layer depletion at pakistan air space. In: *4th International Conference on Recent Advances in Space Technologies*; 2009. p.696-699.

[17] Varotsos C. Modern computational techniques for environmental data; application to the global ozone layer. In: *International Conference on Computational Science*. Berlin, Heidelberg: Springer; 2005. p.504-510.

[18] Jiménez-Hornero FJ, Gutiérrez de Ravé E, Ariza-Villarverde AB, Giráldez JV. Description of the seasonal pattern in ozone concentration time series by using the strange attractor multifractal formalism. *Environmental Monitoring and Assessment*. 2010; 160: 229-236.

[19] Baranowski P, Krzyszczak J, Slawinski C, Hoffmann H, Kozyra J, Nieróbca A, et al. Multifractal analysis of meteorological time series to assess climate impacts. *Climate Research*. 2015; 65: 39-52.

[20] Chakraborty S, Chattopadhyay S. A probe into the behaviour of total ozone time series through multifractal detrended fluctuation analysis. *Theoretical and Applied Climatology*. 2022; 148(1): 671-677.

[21] Drozdz S, Oswiecimka P. Detecting and interpreting distortions in hierarchical organization of complex time series. *Physical Review E*. 2015; 91(3): 030902.

[22] Jaroszewicz S, Mariani MC, Tweneboah OK, Beccar-Varela MP. Multifractal analysis of the southern oscillation index. *Journal of Atmospheric and Solar-Terrestrial Physics*. 2024; 254: 106161.

[23] Salazar-Carballo PA, Ogunjo S, Hernández F, Rodríguez-Marrero JL, Catalán-Acosta A, López-Pérez M. Time series analysis of a 22-year record of 7Be, 210Pb and gross alpha activities in the Canary Islands (Spain) using principal component and multifractal detrended fluctuation analyses. *Science of The Total Environment*. 2024; 942: 173637.

[24] Halder B, Chattopadhyay S, Chattopadhyay G. A detrended fluctuation analysis to examine the pollutant pattern over Gangetic West Bengal of India. *The European Physical Journal Plus*. 2024; 139(9): 827.

[25] Zhao H, He H, Wu C, Zhu X, Zhou D, Peng Z. Multifractal property change of NO_x and O_3 variations in port area in responding to COVID-19 lockdown. *Stochastic Environmental Research and Risk Assessment*. 2024; 38(3): 1145-1161.

[26] Devi RR, Chattopadhyay S. Multifractal detrended fluctuation analysis approach to the monthly total ozone concentration over New Delhi, India. *Indian Journal of Physics*. 2024; 28: 1-7.

[27] Plocoste T, Pavón-Domínguez P, Sankaran A, Euphrasie-Clotilde L. Investigation of $PM_{2.5}$ and PM_{10} dynamics in the caribbean basin using a multifractal framework. *Water, Air, & Soil Pollution*. 2024; 235(11): 732.

[28] Priyanka TMC, Gowrisankar A. Multifractal analysis of fractal interpolation functions. *Physica Scripta*. 2024; 99(11): 115230.

[29] Priyanka TMC, Gowrisankar A, Banerjee S. Mpox outbreak: Time series analysis with multifractal and deep learning network. *Chaos: An Interdisciplinary Journal of Nonlinear Science*. 2024; 34(10): 101103.

[30] Pavón-Domínguez P, Jiménez-Hornero FJ, Gutiérrez de Ravé E. Joint multifractal analysis of the influence of temperature and nitrogen dioxide on tropospheric ozone. *Stochastic Environmental Research and Risk Assessment*. 2015; 29: 1881-1889.

[31] Jiang ZQ, Xie WJ, Zhou WX, Sornette D. Multifractal analysis of financial markets: A review. *Reports on Progress in Physics*. 2019; 82(12): 125901.

[32] Meenakshi M, Gowrisankar A. Fractal-based approach on analyzing the trends of climate dynamics. *International Journal of Modern Physics B*. 2024; 38(30): 2440006.

[33] Qian B, Rasheed K. Hurst exponent and financial market predictability. In: *IASTED Conference on Financial Engineering and Applications*. Cambridge, MA; 2004. p.203-209.

[34] Banerjee S, Hassan MK, Mukherjee S, Gowrisankar A. *Fractal Patterns in Nonlinear Dynamics and Applications*. CRC Press; 2020.

[35] Kavitha C, Meenakshi M, Gowrisankar A. Classification of COVID-19 time series through hurst exponent and fractal dimension. In: Banerjee S, Gowrisankar A. (eds.) *Fractal Signatures in the Dynamics of an Epidemiology: An Analysis of COVID-19 Transmission*. CRC Press; 2004. p.147-161.

[36] Bassingthwaighte JB, Raymond GM. Evaluating rescaled range analysis for time series. *Annals of Biomedical Engineering*. 1994; 22: 432-444.

[37] Mandelbrot BB. Possible refinement of the lognormal hypothesis concerning the distribution of energy dissipation in intermittent turbulence. In: *Statistical Models and Turbulence: Proceedings of a Symposium held at the University of California, San Diego (La Jolla)*. Berlin, Heidelberg: Springer; 2005. p.333-351.

[38] Mandelbrot BB. Multifractal measures, especially for the geophysicist. In: Christopher H, Scholz, Benoit BM. (eds.) *Fractals in Geophysics*; 1989. p.5-42.

[39] Mandelbrot BB. Negative fractal dimensions and multifractals. *Physica A: Statistical Mechanics and its Applications*. 1990; 163(1): 306-315.

[40] Falconer KJ. The multifractal spectrum of statistically self-similar measures. *Journal of theoretical Probability*. 1994; 7: 681-702.

[41] Mandelbrot BB. Intermittent turbulence in self-similar cascades: divergence of high moments and dimension of the carrier. In: *Multifractals and 1/f Noise: Wild Self-Affinity in Physics (1963−1976)*. New York, NY: Springer; 1999. p.317-357.

[42] Kantelhardt JW, Zschiegner SA, Koscielny-Bunde E, Havlin S, Bunde A, Stanley HE. Multifractal detrended fluctuation analysis of nonstationary time series. *Physica A: Statistical Mechanics and its Applications*. 2002; 316(1-4): 87-114.

[43] Ramasamy U, Arulprakash G. Mid-sagittal plane detection in brain magnetic resonance image based on multifractal techniques. *IET Image Processing*. 2016; 10(10): 751-762.

[44] Feder J. Multifractal measures. In: *Fractals*. Boston, MA: Springer; 1988. p.66-103.

[45] Banerjee S, Gowrisankar A, Reddy KM. *Fractal Patterns with MATLAB*. Springer; 2023.

[46] Ihlen EA. Introduction to multifractal detrended fluctuation analysis in Matlab. *Frontiers in physiology*. 2012; 3: 141.

[47] Asuero AG, Sayago A, González AG. The correlation coefficient: An overview. *Critical Reviews in Analytical Chemistry*. 2006; 36(1): 41-59.

[48] Yu H, Hutson AD. Inferential procedures based on the weighted Pearson correlation coefficient test statistic. *Journal of Applied Statistics*. 2024; 51(3): 481-496.

[49] Ritchie H, Rodés-Guirao L, Roser M. Ozone layer. *Our World in Data*. 2023. Available from: https://ourworldindata.org/ozone-layer [Accessed 5th Apr 2023].

[50] Copernicus Climate Change Service (C3S). *CDS Application*; 2024. Available from: https://cds.climate.copernicus.eu/cdsapp [Accessed 22nd March 2024].

[51] National Aeronautics and Space Administration and Goddard Space Flight Center. *Ozone 2023 MERRA2 Southern Hemisphere*; 2024. Available from: https://ozonewatch.gsfc.nasa.gov/meteorology/ozone_2023_MERRA2_SH.html [Accessed 5th April 2024].

[52] Zhou WX. Multifractal detrended cross-correlation analysis for two nonstationary signals. *Physical Review E-Statistical, Nonlinear, and Soft Matter Physics*. 2008; 77(6): 066211.

[53] Jiang ZQ, Zhou WX. Multifractal detrending moving-average cross-correlation analysis. *Physical Review E*. 2011; 84(1): 016106.

[54] Oswiecimka P, Drozdz S, Forczek M, Jadach S, Kwapien J. Detrended cross-correlation analysis consistently extended to multifractality. *Physical Review E*. 2014; 89(2): 023305.